

## Direct power control based virtual flux using SOGI-FLL estimator for BDFIG-WEC system

Abderrezak Rahab<sup>\*</sup>, Fawzi Senani<sup>†</sup> and Hocine Benalla

Laboratoire de l'Electrotechnique de Constantine, LEC  
Faculté des Sciences de la Technologie  
Université des frères Mentouri de Constantine 1  
Ain El-bey 25000 Constantine, Algérie

(reçu le 30 Août 2017 - accepté le 30 Septembre 2017)

**Abstract** – *This paper deals with the control aspect of the brushless doubly fed induction generator, 'BDFIG' incorporating in a wind energy conversion system, 'WECS'. The control process may divide in two main parts control of machine side converter, 'MSC' and grid side converter, 'GSC'. Control process adopts direct power control, DPC approach thanks to its robustness and implementation simplicity direct power control permits decoupled regulation for active and reactive powers and as well pretty good robustness and performance during transient and steady state operation without PI regulators and rotating coordinate transformations. The regulation of power flow toward supply network via stator is performed using conventional direct power control at level the machine side converter where the active power reference signal is tuning depending to the output of the MPPT unit and the reactive power reference signal is set to zero to ensure unity power factor operation. Meanwhile, control of power flow between grid and grid side converter, 'GSC' is done using improved direct power control based virtual flux and Second order generalized integrator - frequency locked loop, 'SOGI-FLL' estimator in order to estimate frequency and angular position of voltage grid vector and as well power flow has been analysed during various operation conditions, 'synchronous, sub synchronous and super synchronous speeds'. The obtained simulation results show satisfactory system operation in terms of robustness and optimum power tracking behaviour and good steady state stability and finally reasonable settling time during transients.*

**Résumé** - *Cet article traite de la commande du générateur à induction brushless doublement alimenté, 'BDFIG' en incorporant un système de conversion d'énergie éolienne, 'WECS'. Le procédé de commande peut être divisé en deux parties, la commande du convertisseur côté machine 'MSC' et le convertisseur côté réseau 'GSC'. Le procédé de commande adopte une commande directe de puissance 'DPC' en raison de sa robustesse et la facilité de son implémentation permet la régulation découplée pour les puissances actives et réactives, ainsi qu'une bonne robustesse et de bonnes performances en régime transitoire et stationnaire sans régulateurs PI et en transformations de coordonnées en rotation. La régulation du flux de puissance vers le réseau d'approvisionnement via un stator est réalisé en utilisant un DPC conventionnel au niveau du MSC ou le signal de référence de la puissance active est mis au point en fonction de la sortie du MPPT et le signal de référence de puissance réactive est réglé à zéro pour assurer des opérations de facteurs de puissance unitaires. En même temps, la commande du flux de puissance entre le réseau et le GSC est réalisé en utilisant un DPC amélioré basé sur un flux virtuel et un intégrateur généralisé de second ordre-boucle verrouillée en fréquence 'SOGI-FLL' afin d'estimer la fréquence et la position angulaire du vecteur de tension du réseau, aussi, le flux de puissance a été analysé dans différentes conditions opératoires: à des vitesses synchrones, sous synchrones, et super synchrones. Les résultats de simulations qui ont été obtenus ont montré que le système opérait de manière satisfaisante en terme de robustesse et de tracking du point de puissance*

---

\* rahababderzzak@gmail.com

† senani.fouzi@gmail.com - benalladz@yahoo.fr

*optimum, et possède une bonne stabilité en régime stationnaire et un temps d'installation raisonnable durant les régimes transitoires.*

**Keywords:** Wind energy conversion system - BDFIG - MPPT control - Direct power control, DPC - SOGI-FLL - Virtual Flux Estimation.

## 1. INTRODUCTION

Wind power has become increasingly popular because of the increasing difficulty of the pollution of the Environment. Enormous efforts have been put in the advancement of WECS, to reduce costs, increase the efficiency and the reliability [1-2], with the sustained and rapid growth of world economy, the energy demand is increasing day by day, but a large amount of fossil fuel is used to lead to the environmental pollution aggravation.

The wind energy as a clean and renewable energy accords with the future energy development [3]. The permanent magnet synchronous generator and the doubly fed induction generator based of WECS 'PMSG WECS', 'DFIG-WECS' has become the most popular configuration for wind energy applications on one hand, the DFIG has several advantages including the maximum power capture over a wide speed range and decoupled active and reactive power control. It also allows the use of a partially rated converter which reduces the system cost [2, 4]. The use of brushes and slip rings associated with the rotors of DFIG decreases the robustness of system and increases the maintenance cost [2, 5, 6].

The cost of maintenance for traditional DFIG based wind generators increased the pressure to seek other alternative generator systems. Brushless doubly-fed machines are the evolution of the cascaded induction machine and can be widely used for medium and large wind turbines with limited speed ranges [2-5].

The 'BDFIG', also known as a self-cascaded generator, is composed of two stator of different pole numbers called stator of power winding 'PW' and stator of control winding, 'CW' and a special rotor winding. Normally the two stator supplies are of various frequencies, one a fixed frequency supply linked to the grid via converter, and the other a variable frequency supply derived from two-level bidirectional converters AC-DC-AC as illustrated in figure 1.

The converters capacity in the control winding are of almost 25 % of the machines rated power, which can operate in a wide speed range including super-synchronous, synchronous and sub-synchronous [4, 7-11], a medium speed machine, enabling the use of a simplified one or two stage gearbox, excluding the third high-speed stage, known to be the highest failure rate part of the gearbox, hence reducing the weight of the overall drive train and further improving reliability, reduced capital and maintenance costs and has significantly greater LVRT capability [9, 10].

The 'BDFIG-WECS' retains all the advantages of 'DFIG-WECS' and improves reliability by removing brushes and slip rings. Therefore, the 'BDFIG-WECS' shows great potential in future wind power generation, especially the large wind turbines and offshore wind farm where maintenance costs are high. [12-13].

'BDFIG' modeling is much more complex, which makes quite difficult control system design. Various strategies of control have been used to control of machine side converter, 'MSC' {the scalar current control, direct torque control, fuzzy power control, sliding mode power control, and flux oriented control based on rotor flux or stator flux/voltage orientation} [12].

At present, the vector control is mainly adopted to implement the power decoupling control of 'BDFG' [7, 11, 14]. But the vector control requires the complicated control

algorithm and high performance processor, and greatly depends on the 'BDFG' parameters, which leads to the poor robustness of the system [4]. The direct torque control, 'DTC' with the simpler control algorithm, faster dynamic response and better robustness than the vector control has been attempted to apply for the variable-speed constant-frequency 'BDFG' control system [4-6].

But the flux observer of 'DTC' is sensitive to the generator parameter variation and inaccurate identification, which leads to the bad real-time of control system. Alternatively, the direct power control, 'DPC', derived from DTC, can directly decouple and independently control the active and reactive powers to implement the power tracking. DPC has a simpler algorithm and less calculation than DTC, and does not need to observe the flux amplitude, which can well solve the problem of the bad real-time of control system caused by the flux observer being sensitive to generator parameter variations. Therefore, 'DPC' of 'MSC' has been applied to the 'BDFIG' control system [3-5, 12], the three strategies are based on the same principle with the only difference existing in flux estimation algorithm.

The grid side converter, 'GSC' control approaches can be classified, as cited in the literature as a vector oriented control, 'VOC' and direct power control 'DPC' [13], the vector control, 'VC' can be either based on grid voltage [14-16] or virtual-flux [17] using proportional-integral (PI) controllers. However, it has some disadvantages, such as its dependence on the system parameters variation, that its performance largely depends on the tuning of the PI parameters [18].

In order to overcome complication due to the current control loops, an effective control, namely direct power control, DPC has been developed [19], Direct power control, DPC strategy has become one of the hot research topics in recent Years, because of its fast dynamic response, simple structure, and high power factor, and so on [20, 21]. In general, the control of 'GSC' converter contains more sensors {DC voltage sensor, power grid voltage sensors and AC current sensors}, which not only increases the volume of the system device, improves the system cost, but also reduces the system reliability of 'GSC' [21].

The 'GSC' can be seen as a virtual AC motor, its virtual flux-linkage can be used to estimate the voltage of 'GSC', but in the conventional virtual flux estimation of 'GSC' converter, there exists a pure integral link, and then the estimation process of virtual flux is inevitably affected by the initial value and the cumulative deviation of the integrator [21-27].

The resolution of the problems of pure integration, more researchers focus on replacing the pure integrator by using low-pass filters, 'LPFs', the initial value problem of pure integrator can be successfully solved [21, 25-27], however, the problem of amplitude and phase deviation is caused.

In order to overcome the influence of integral initial value and cumulative deviation of pure integrator, and avoid the amplitude and phase deviation caused by first-order low-pass filter, this paper proposes a new method for Virtual Flux estimation that is inherently capable of handling these problems, as a result a stable and smooth virtual flux estimated and sector detection with precision. The suggested method is based on utilizing the Second Order Generalized Integrator, 'SOGI' from [24-26].

This paper is organized as follows- In Section 2, the description basic principles of system, 'BDFIG-WEC' chain studied. In Section 3, the mathematical model of 'BDFIG', Wind Turbine and three-phase grid side converter, 'GSC' are derived. In Section 4, presents controls of different parts of the 'WEC' chain, DPC method is used to control of machine side converter, 'MSC' of 'BDFIG', the maximum power point tracking, 'MPPT' method was implemented for optimal energy capture by the wind turbine, direct power

control based virtual flux estimation, 'VF-DPC' by using Second Order Generalized Integrator frequency located loop, 'SOGI-FLL' of 'GSC' converter to control the voltage of the DC Link is proposed for simplicity ,robustness, and excellent performance. Section 5 presented some simulation results and discussion finally, the conclusion are provided in section 6.

## 2. DESCRIPTION OF SYSTEM 'BDFIG-WEC' CHAIN

The configuration of the 'BDFIG-WEC' is show in figure1 the rotor of the 'BDFIG' is connected to wind turbine, The main stator Power Winding 'PW' has pole pairs 'Pp' connected directly to the grid than the auxiliary stator {control Winding, 'CW'} has pole pairs 'Pc' fed by a variable voltage and frequency converter, which only handles a fraction of the rated power, the 'BDFIG' can operate in several mode ways including synchronous, doubly-fed, asynchronous mode [8]. The synchronous mode of operation of the 'BDFIG' is desirable operation mode, in this mode of operation the shaft speed is independent of the machine torque and is given by:

$$\omega_r = \frac{\omega_p \pm \omega_C}{P_p + P_C} \tag{1}$$

Or

$$N_r = 60 \frac{f_p - f_C}{P_p + P_C} \tag{2}$$

Where,  $\omega_p$ ,  $\omega_C$  are angular frequencies of the supplies to the PW and CW, respectively,  $f_p$  and  $f_C$  are PW and CW supply frequencies,  $P_p$  and  $P_C$  are their pole pair numbers, respectively. The positive and negative signs indicate the sequence of stator control winding excitation with respect to the power winding. With the CW shorted ( $\omega_C = 0$ ) or the control winding is fed with dc current, the shaft speed is defined as the natural speed ( $\omega_n$ ) given by:

$$\omega_n = \frac{\omega_p}{P_p + P_C} \tag{3}$$

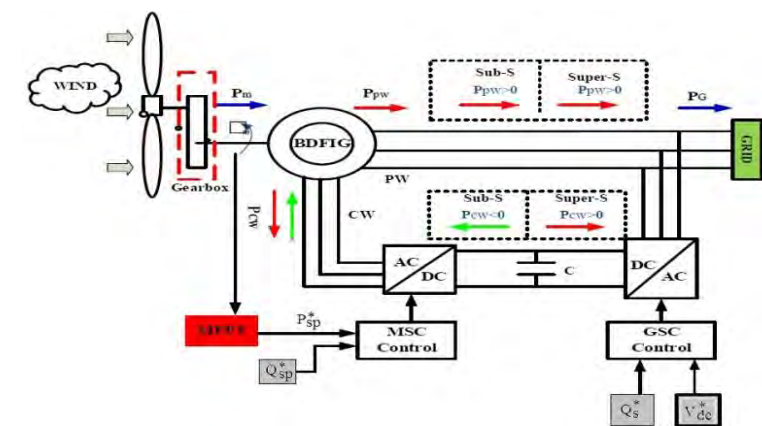


Fig. 1: Schematic diagram of a 'BDFIG' based wind power system

Figure 1 also show de power flow in a lossless 'BDFIG' and are listed in **Table 1**. [8, 10].

**Table 1:** Power Flows in a lossless BDFIG

Generator mode	Speed		
	$0 < \omega_r < \omega_n$	$\omega_n < \omega_r < \omega_p$	$\omega_r > \omega_p$
Power winding, PW	Out	Out	Out
Control winding, CW	Out	In	In

### 3. MODELLING OF THE WECS

#### 3.1 Wind turbine aerodynamic model

In this paper, we are used the same model cited in [28, 29]

The wind power is defined as follows

$$P_v = \frac{1}{2} \pi \rho R^2 v^3 \quad (4)$$

The aerodynamic power  $P_a$  captured by the wind turbine is given by:

$$P_a = \frac{1}{2} \pi \rho R^2 C_p(\lambda, \beta) v^3 \quad (5)$$

The wind turbine is characterized by its curve  $C_p = f(\lambda)$ , figure 2, with  $\lambda$  is the ratio between the tip peripheral speed of blades and the wind speed, in this paper,  $\beta$  is supposed to be zero and so  $C_p$  is only depended to  $\lambda$ .

$$\lambda = \frac{R \omega}{v} \quad (6)$$

$C_p$ , power coefficient,  $\rho$ , density of air (1.25 kg/m<sup>3</sup>),  $v$ , wind speed,  $R$ , turbine rayon.

Increasing  $\beta$  allows the reduction of power coefficient or mechanical power recovered from the axis of the wind turbine show figure 2.

#### 3.2 Mathematical model of 'BDFG'

The model of the 'BDFG' in the PW flux frame is expressed as, [11]:

$$\left\{ \begin{array}{l} v_{qsp} = R_{sp} i_{qsp} + \frac{d\Psi_{sp}}{dt} + \omega_p \Psi_{dsp} \\ v_{dsp} = R_{sp} i_{dsp} + \frac{d\Psi_{dsp}}{dt} - (\omega_p - (P_p + P_c) \omega_r) \Psi_{qsp} \\ v_{dsc} = R_{sc} i_{dsc} + \frac{d\Psi_{dsc}}{dt} - (\omega_p - (P_p + P_c) \omega_r) \Psi_{qsc} \\ v_{qsc} = R_{sc} i_{qsc} + \frac{d\Psi_{qsc}}{dt} + (\omega_p - (P_p + P_c) \omega_r) \Psi_{dsc} \\ 0 = R_r i_{dr} + \frac{d\Psi_{dr}}{dt} - (\omega_p - P_p \omega_r) \Phi_{qr} \\ 0 = R_r i_{qr} + \frac{d\Psi_{qr}}{dt} + (\omega_p - P_p \omega_r) \Phi_{dr} \end{array} \right. \quad (7)$$

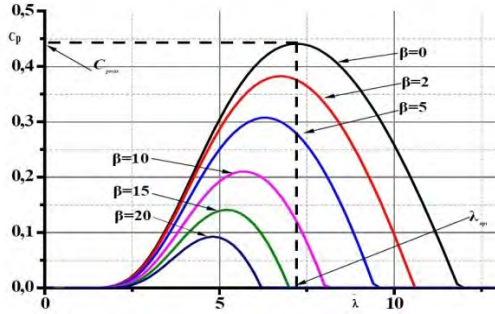


Fig. 2: Power coefficient vs tip speed ratio

$$\begin{cases}
 \Psi_{dsp} = L_{sp} i_{dsp} + M_{spr} i_{dr} \\
 \Psi_{qsp} = L_{sp} i_{qsp} + M_{spr} i_{qr} \\
 \Psi_{dsc} = L_{sc} i_{dsc} + M_{scr} i_{dr} \\
 \Psi_{qsc} = L_{sc} i_{qsc} + M_{scr} i_{qr} \\
 \Psi_{dr} = L_r i_{dr} + M_{scr} i_{dsc} + M_{spr} i_{dsp} \\
 \Psi_{qr} = L_r i_{qr} + M_{scr} i_{qsc} + M_{spr} i_{qsp}
 \end{cases} \tag{8}$$

The aerodynamic torque is given by:

$$C_{em} = p_p M_{spr} \cdot (i_{qsp} i_{dr} - i_{dsp} i_{qr}) + p_c M_{scr} \cdot (i_{dsc} i_{qr} - i_{qsc} i_{dr}) \tag{9}$$

According to the instantaneous power theory, the active and reactive powers of the (PW) are defined as:

$$P_{sp} \equiv \frac{3}{2} (V_{sdp} \cdot I_{sdp} + V_{sqp} \cdot I_{sqp}) \tag{10}$$

$$Q_{sp} \equiv \frac{3}{2} (V_{sqp} \cdot I_{sdp} + V_{sdp} \cdot I_{sqp}) \tag{11}$$

### 3.3 Model of three-phase PWM converter 'GSC & MSC'

The main objective of grid side converter 'GSC' is to keep the dc-link voltage constant it is controlled using a 'VF-DPC' based SOGI flux estimation.

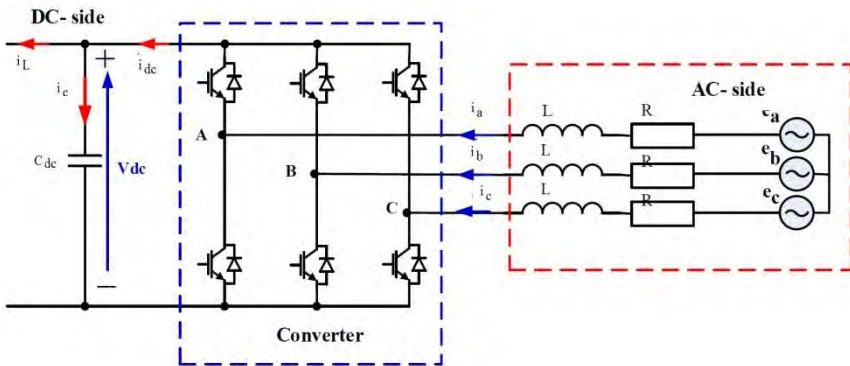


Fig. 3: Block diagram for three-phase PWM rectifier

The converter can be expressed, in a-b-c reference frame with following equations [20]:

$$\begin{bmatrix} e_a \\ e_b \\ e_c \end{bmatrix} \equiv R \begin{bmatrix} e_a \\ e_b \\ e_c \end{bmatrix} + L \frac{d}{dt} \begin{bmatrix} I_a \\ I_b \\ I_c \end{bmatrix} + \begin{bmatrix} V_a \\ V_b \\ V_c \end{bmatrix} \quad (12)$$

Where,  $L$  and  $R$  are the inductance and resistance of the chokes, respectively  $e_a$ ,  $e_b$ ,  $e_c$ ,  $i_a$ ,  $i_b$  and  $i_c$  are the electrical grid voltage and current,  $V_A$ ,  $V_B$ ,  $V_C$  are the AC side voltages of the converter,

The AC rectifier's voltages  $V_A$ ,  $V_B$ ,  $V_C$  are defined as:

$$\begin{cases} V_A - \frac{V_{dc}}{3}(2S_a - S_b - S_c) \\ V_B - \frac{V_{dc}}{3}(-S_a + 2S_b - S_c) \\ V_C - \frac{V_{dc}}{3}(-S_a - S_b + 2S_c) \end{cases} \quad (13)$$

$S_a$ ,  $S_b$  and  $S_c$  are the switching states of the rectifier show figure 8.

The relationship between the AC side rectifier currents  $i_a$ ,  $i_b$  and  $i_c$  and the DC bus voltage  $V_{dc}$  can be written.

$$C_{dc} \frac{dV_{dc}}{dt} \equiv S_a i_a + S_b i_b + S_c i_c - i_L \quad (14)$$

Where  $C_{dc}$  is the dc link capacitance,  $i_L$  the load current.

## 4. CONTROL OF THE 'BDFIG-WECS' CHAIN

### 4.1 Maximum power point tracking technique

Maximum power point tracking 'MPPT' strategies play an important role in wind power conversion systems 'WECS' because they maximize the power extracted from the wind, and therefore optimize the conversion efficiency.

Figure 4 shows the Power-Speed characteristics of the wind turbine, the peak power for each wind speed occurs at the point where  $C_p$  is maximized. To maximize the power generated, it is therefore desirable for the generator to have a power characteristic that will follow the maximum  $C_{pmax}$  line.

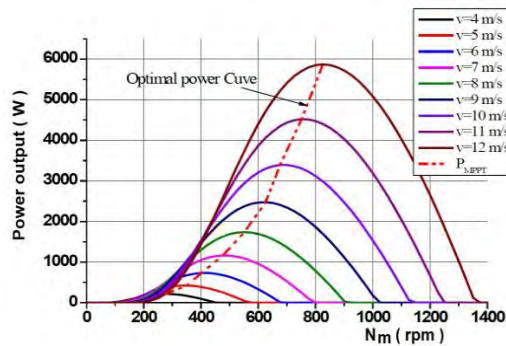


Fig. 4: Characteristics curve of wind turbine ( $\lambda_{opt} \equiv 8.1$ ;  $C_{pmax} \equiv 0.48$ ;  $\beta = 0$ ) [29]

Two strategies are used in literature with or without speed control. In this paper, we used the strategy without speed control; this method is superior to others because of its simplicity and accuracy.

The other advantage of this method is that there is no need to speed controller and wind speed sensor [30, 31].

The simplified representation of wind turbine model without speed control in the form of diagram blocks is given in figure5 [30].

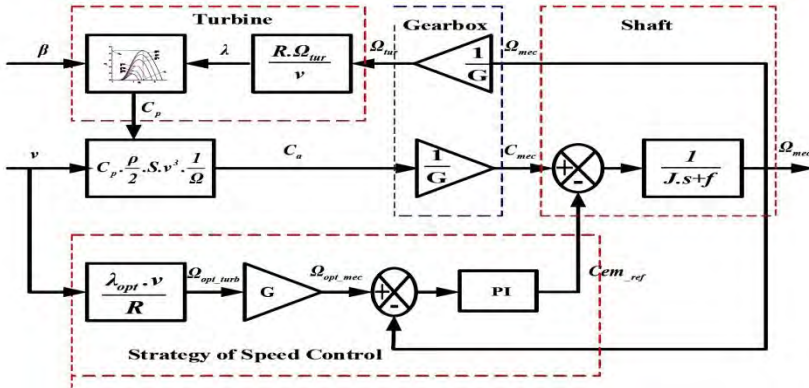


Fig. 5: Wind turbine model without speed control

#### 4.2 Direct power control 'DPC' OF 'BDFIG'

The control idea of DPC is derived from DTC. The DPC principle diagram of the 'BDFIG' is shown as figure 6, which is similar to DTC, the reference active power  $P_{sp}^*$  is set by maximum power tracking strategy according to wind speed. Reference reactive power  $Q_{sp}^*$  is set zero for kept unity power factor,  $dP$  and  $dQ$  are respectively the errors of the active and reactive power.

For a MSC three phase two level inverter, there are eight possible voltage vectors {six active vectors and two null vectors}, and the  $\alpha\beta$  plane is divided into six sectors, as show in figure 7b.

The flux amplitude  $\Psi_{sp}$  of the 'PW' winding is approximately constant due to the power winding is directly connected to the power grid, so the active power  $P_{sp}$  can be controlled by changing the rotational speed and direction of the control winding flux ,  $\Psi_{sc}$ , referring to the DTC method, the reactive power  $\Psi_{sp}$  can be controlled by changing the flux amplitude of the (CW) winding. Therefore, the switching voltage vector selection table has to be re-established according to the error signals of the active and reactive powers as well as the section location information of the 'CW' flux, the active and reactive powers of the 'BDFIG' can be directly decoupled and independently controlled by properly selecting the switching voltage vectors [3].

The power winding 'PW' stator flux and control winding 'CW' stator flux are estimated by (15), (16).

$$\Psi_{sp} = \int (V_{sp} + R_{sp} i_{sp}) dt = \int e_{sp} dt \tag{15}$$

$$\Psi_{sc} = \int (V_{sc} + R_{sc} i_{sc}) dt = \int e_{sc} dt \tag{16}$$

### 4.2.1 Voltage vectors effects on active and reactive powers [4, 5]

In this section, the relation between the voltage vectors of the inverter and the 'BDFIG' output power will be deduced. For three-phase two-level inverters, there are eight possible voltage vectors {six active vectors and two null vectors}, and the  $\alpha-\beta$  plane is divided into six sectors, as shown in figure 7a.

The control diagram of 'DPC' strategy of 'BDFIG' is illustrated in figure 6. The actual output powers  $P_{sp}$  and  $Q_{sp}$  are first estimated, and then compared with the references  $P_{ref}$  and  $Q_{ref}$ . The errors are sent to two fixed band hysteresis comparators to produce digitized signals  $dP$  and  $dQ$ . Finally, the voltage vector is selected from Table 2 according to  $dP$ ,  $dQ$  and the position of  $\Psi_{sc}$ .

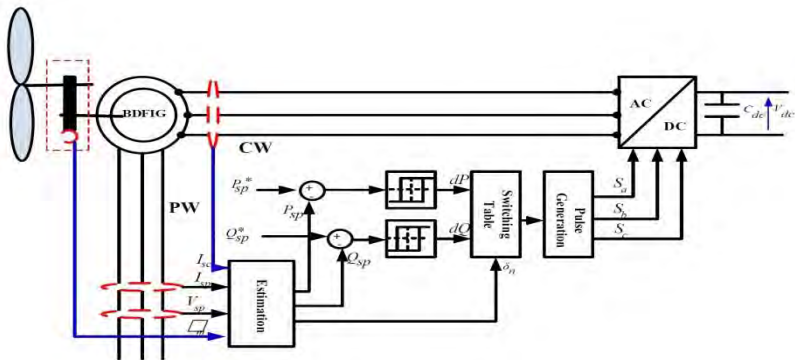


Fig. 6: Block diagram of DPC controller for 'CBDFIGs'

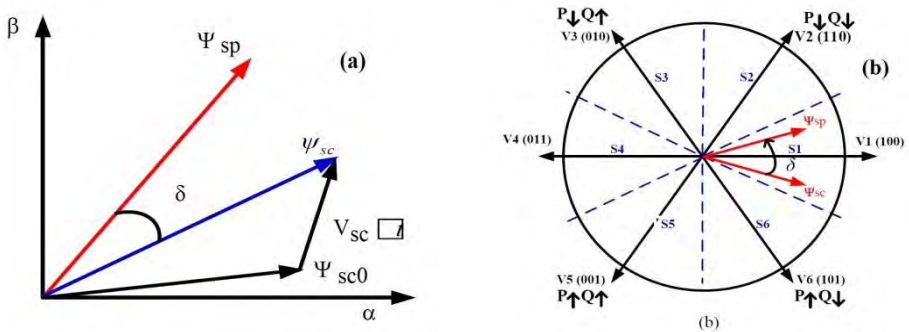


Fig. 7: (a) Relationship between voltage vector and flux vector (b) Voltage vectors generated by the inverter and sector division

### 4.2.2 'CW' flux estimation

Flux estimation plays an important role in high-performance electrical drive systems, including those based on field oriented control 'FOC' and direct control 'DPC' and 'DTC'. The three 'DPC' strategies of brushless doubly fed induction generator realized in [4, 5, 12] respectively, are based on same principle with the only difference existing in flux estimation algorithm.

In note 'DPC' strategies in [12], high reliability with the elimination of rotor current/position sensor and rotating coordinate transformation, and less parameter independent with the control machine stator resistance.

The 'CW' stator flux can be obtained by integrating the back electromotive force '  $e_{sc}$  ' equation (16), however, it is well know that a pure integrator suffers from three main problems the first related to dc drift, when integrated, will cause the integrator to saturate, the second is caused by the initial condition of integration, may lead to a dc offset at the output of the integrator.

The third related to harmonics, more detailed in [25, 26]. Based the same principle DPC strategies, in this paper a new flux estimation method based on the second order generalized integrator frequency-locked loop 'SOGI-FLL' are presented. More detail for this method presented in next part.

**Table 2:** The voltage vector control selection table [3, 31]

Error		Section					
$dP$	$dQ$	$\delta_1$	$\delta_2$	$\delta_3$	$\delta_4$	$\delta_5$	$\delta_6$
0	0	$V_6$	$V_1$	$V_2$	$V_3$	$V_4$	$V_5$
1	0	$V_2$	$V_3$	$V_4$	$V_5$	$V_6$	$V_1$
0	1	$V_5$	$V_6$	$V_1$	$V_2$	$V_3$	$V_4$
1	1	$V_3$	$V_4$	$V_5$	$V_6$	$V_1$	$V_2$

**4.3 Virtual flux based direct power control 'VF-DPC' for 'GSC'**

The virtual flux 'VF' concept which relates the grid voltage and the ac-side inductors to a virtual ac motor is shown in figure 9a hence; R and L represent the stator resistance and the stator leakage resistance of the virtual motor. The line-to-line grid voltages  $e_{ab}$ ,  $e_{bc}$ ,  $e_{ca}$  would be induced by a virtual air-gap flux. In other perspective, the integration of the line voltages leads to a virtual line vector  $\Psi_L$ . Figure 8 shows the basic scheme of 'VF-DPC'.

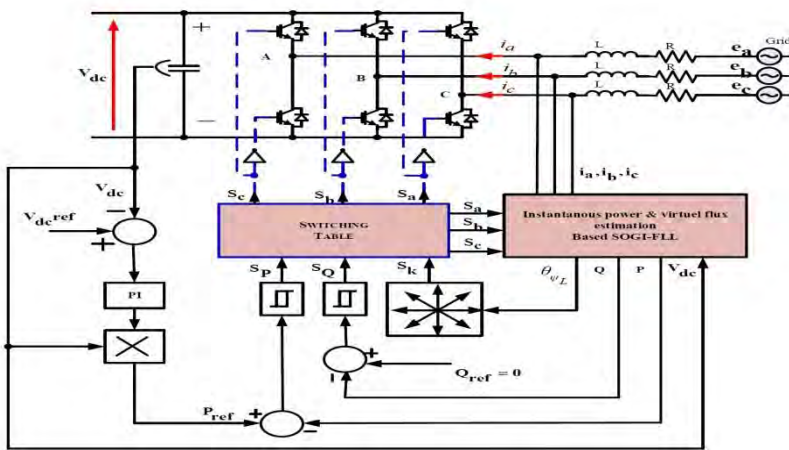


Fig. 8: Virtual-flux based direct power control 'VF-DPC' scheme

The command active power  $P_{ref}$  and reactive power  $Q_{ref}$  are compared with the estimated P and Q values via active and reactive power hysteresis controllers, respectively.

The digitized output signals  $S_p$  and  $S_q$  and the VF vector position ( $\theta$ ) are used to select the appropriate voltage vector according to the switching table defined in [19].

### 4.3.1 Power estimation based on virtual flux

Figure 9a shows a single phase equivalent circuit of the virtual motor that is connected to the point of common coupling of the converter. The line voltage  $e_L$  represents the machines Electromotive force.

The mains virtual flux 'VF' calculation is based on flux definition (17) and the voltage loop equation (18).

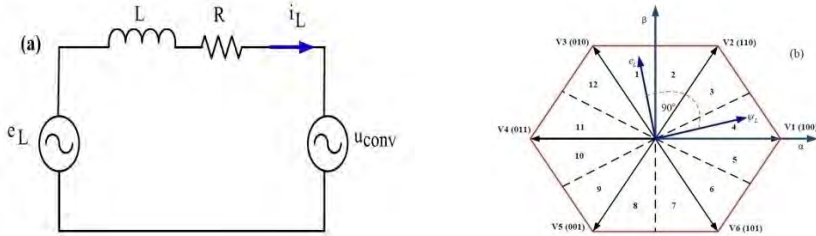


Fig. 9: (a) Single phase equivalent circuit of mains connected three-phase rectifier, (b) Sector selection for 'VF-DPC' technique [20]

$$\Psi_L = \int e_L dt \quad (17)$$

$$e_L = u_{conv} + R i_L + L \frac{d}{dt} i_L \quad (18)$$

In practice,  $R$  can be neglected which gives hence, the line virtual flux vector  $\Psi_L$  can be calculated based on the measured line current  $i_L$  and the converter voltage  $u_{conv}$ .

Based on the measured dc-link voltage  $V_{dc}$  and the converter switch states  $S_a$ ,  $S_b$  and  $S_c$ , the rectifier voltages are estimated in as follows [19]:

$$u_{conv\alpha} = \sqrt{\frac{2}{32}} U_{dc} \left( S_a - \frac{1}{2}(S_b + S_c) \right) \quad (19)$$

$$u_{conv\beta} = \frac{1}{\sqrt{2}} U_{dc} (S_b + S_c) \quad (20)$$

The virtual flux components are calculated in stationary ( $\alpha - \beta$ ) coordinates system as:

$$\Psi_{L\alpha} = \int \left( u_{conv\alpha} + L \frac{di_{L\alpha}}{dt} \right) dt \quad (21)$$

$$\Psi_{L\beta} = \int \left( u_{conv\beta} + L \frac{di_{L\beta}}{dt} \right) dt \quad (22)$$

Then, equations (23) and (24) are used to estimate the active and reactive power [20].

$$P = \omega(\Psi_{L\alpha} i_{L\beta} - \Psi_{L\beta} i_{L\alpha}) \quad (23)$$

$$Q = \omega(\Psi_{L\alpha} i_{L\alpha} - \Psi_{L\beta} i_{L\beta}) \quad (24)$$

The VF vector position  $\theta_{\Psi_L} = \tan^{-1}(\Psi_{L\alpha}/\Psi_{L\beta})$  is used in 'VF-DPC' scheme to select the appropriate converters voltage vector according to the switching table defined in [32].

**4.3.2 'SOGI-FLL' flux estimation**

**a. Structure du 'SOGI'**

The structure of the SOGI is shown on figure 10a the first output ( $u'$ ) of the SOGI is in phase and with the same amplitude with the input ( $u$ ), the second output ( $qu'$ ) is shifted of  $90^\circ$  with the same amplitude, (the letter 'q' is for indicating that this output is in quadrature with ( $u'$ ) the two output can then be used for computing magnitude and phase of input ( $u$ ).  $k$  is the damping factor of the filter, a gain of great value gives a quick response but can affect the accuracy of the filter and a gain of low value can cause a very long transient response. Then, taking into account all these circumstances the value optimal of gain  $k$  is ( $\sqrt{2}$ ) [24, 25].

$$D(S) = \frac{u'}{u}(S) = \frac{k \omega' S}{S^2 + k \omega' S + \omega'^2} \tag{25}$$

$$Q(S) = \frac{qu'}{u}(S) = \frac{k \omega'^2}{S^2 + k \omega' S + \omega'^2} \tag{26}$$

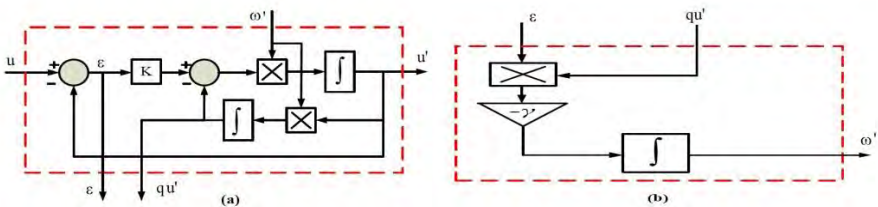


Fig. 10: Block diagram (a) 'SOGI-QSG' scheme, (b) 'FLL Block'

The transfer functions represented by (25) and (26) for band pass filter 'BPF' and low-pass filter 'LPF', respectively. The bandwidth of the 'BPF'  $D(s)$  and 'LPF'  $Q(s)$ , can be adjusted by proper tuning of the real positive value of gain  $k$ . Hence, the signals  $u'$  and  $qu'$  are the outputs of the BPF and LPF, respectively, with  $90^\circ$  phase shift between them show figure11, where the ( $\omega'$ ) sets the centre frequency (nominally 50 Hz).

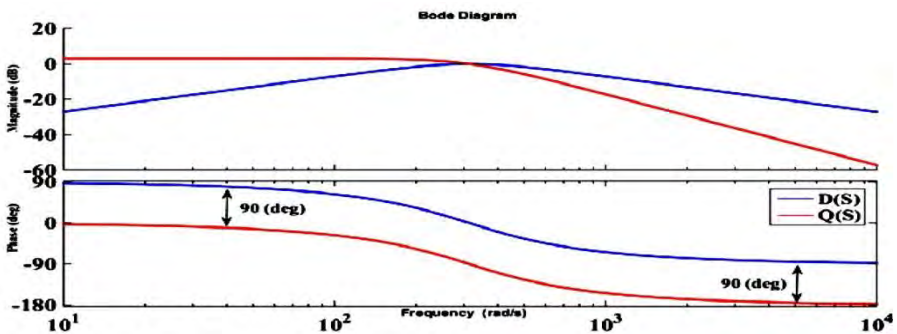


Fig. 11: 'SOGI' bode plot: (a)  $D(s)$  for different values of 'k'

(b)  $D(s)$  and  $Q(s)$  for  $k = \sqrt{2}$  and  $\omega' = 2\pi 50$

**b. Frequency-locked loop 'FLL'**

The introduction of the FLL allows to adapt the input frequency of the 'SOGI' with the frequency of the signal is filtered.

Of this fact, the analysis of the transfer function of the error ( E ) compared to the input signal ( u ) is essential:

$$E(S) = \frac{\varepsilon}{u}(S) = \frac{S^2 + \omega'^2}{S^2 + k\omega'S + \omega'^2} \tag{27}$$

The transfer function of (27) resembles a filter passes band with a null (gain) at the frequency (  $\omega'$  ), the Bode diagram of (26) and (27) are represented in figure 12.

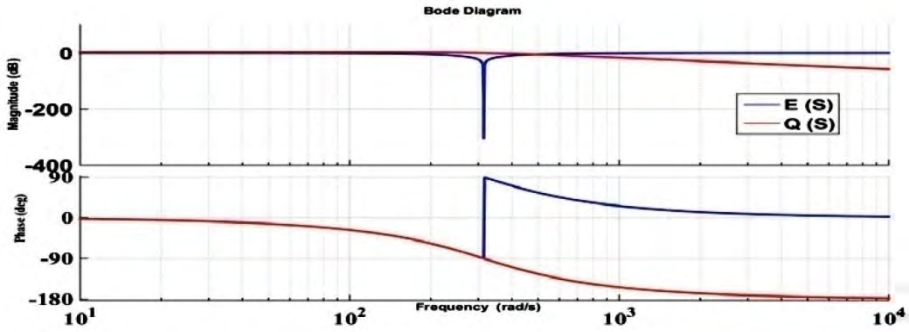


Fig. 12: 'SOGI' bode plot: E(s) and Q(s) for  $k = \sqrt{2}$  and  $\omega' = 2\pi 50$

According to the figure 12, it is clear that the error signal and the component in quadrature is in phase when ( $\omega < \omega'$ ) and it is in reverse of phase when ( $\omega > \omega'$ ). Defining anew variable equal to the product of the error (  $\varepsilon$  ) by the signal in quadrature (  $qu'$  ), the average value of this new variable is positive when ( $\omega < \omega'$ ), zero when ( $\omega = \omega'$ ), and negative when ( $\omega > \omega'$ ). Therefore a regulator with a negative gain is sufficient to eliminate the DC component of the frequency error By shifting the frequency a shown figure10b.

In order to overcome the disadvantage to the use of filters in cascade to estimate the virtual flows under a network unbalanced and full of harmonics {The delay, sensitivity to the variation of the frequency of the network, a dynamic and very slow}, The 'SOGI' account as a good solution for the estimation of the Virtual flux Under a disturbed network.

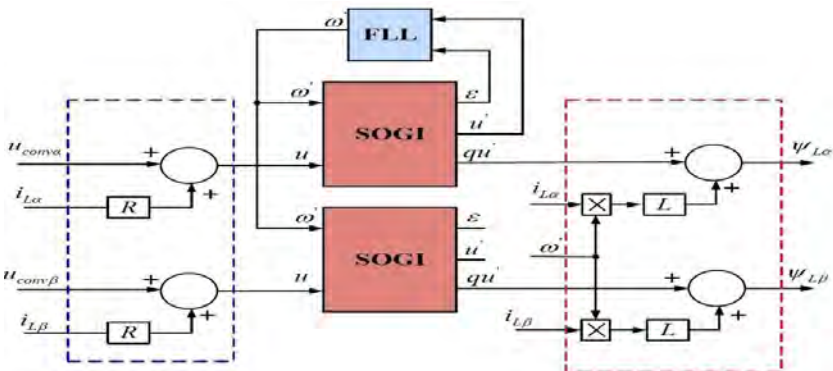


Fig. 13: Estimation of the virtual flow by SOGI under ideal source

As already seen previously, the second output of the 'SOGI' is a signal of the same amplitude to that of the input but shift of  $90^\circ$ , So we can use the 'SOGI' to integrate (21), (22) and by consequence estimate the virtual flux [24]. Under a balanced network, the virtual flux can be estimated by the 'SOGI' as illustrated in figure 13.

### 5. SIMULATION RESULTS

For the validation of the proposed 'DPC' strategy, the system has been modelled and built in Matlab/Simulink software environment and tested under various conditions. The 'BDFIG' based system is about 2 taken about 100 kHz. The converter dc link voltage is set at 600 V. The control of grid side converter, 'GSC' aims to maintain a constant dc-link voltage, and it is controlled using 'VF-DPC' method based 'SOGI-FLL' virtual flux estimator. The machine side converter, 'MSC' is exploited to regulate the power flow via 'BDFIG' stator to the grid using conventional 'DPC' strategy.

In order to verify the good performance 2.5 kW power scale and its parameters are given in [11]. The sampling frequency during simulation is and advantages offered by control combination of 'DPC-BDFIG' machine for 'MSC' and 'VF-DPC-SOGI-FLL' for GSC, starting procedure is not relevant to this paper and not shown in the results.

The system is analysed during steady-state and transients conditions at two case, wind step change (sub-synchronous, synchronous and super-synchronous) operation figure 14a and variable wind profile figure 14b.

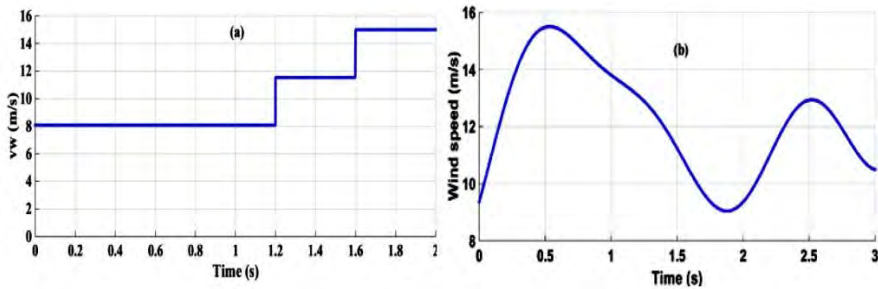


Fig. 14: Wind speed (a) Step change (b) Variable wind profile

#### 5.1 Simulation case 1: results with step change of wind power

The wind speed steps from 8.12 m/s to 11.8 m/s at instant 1.2 s, and from 11.8 m/s to 15 m/s at instant 1.6 s as shown in figure 14a. According to the corresponding optimal speed of 'BDFIG' machine is 525 tr/min at the start up, 750 tr/min at instant 1.2 s, and 975 tr/min at instant 1.6 s as shown in figure 15a.

##### 5.1.1 Simulation result of 'DPC-BDFIG' for 'MSC'

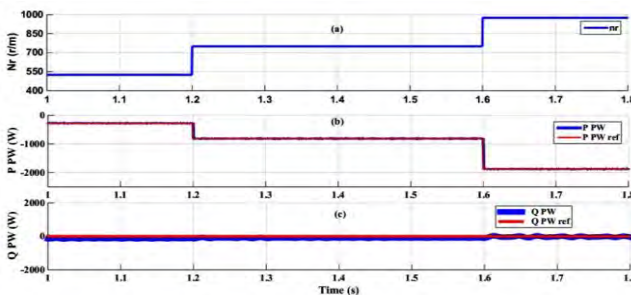


Fig. 15: Simulation results of 'DPC-BDFIG' of 'MSC' under speed step

{super-synchronous mode, synchronous mode, sub-synchronous mode}  
 (a) Speed; (b) PW active power; (c) PW active power

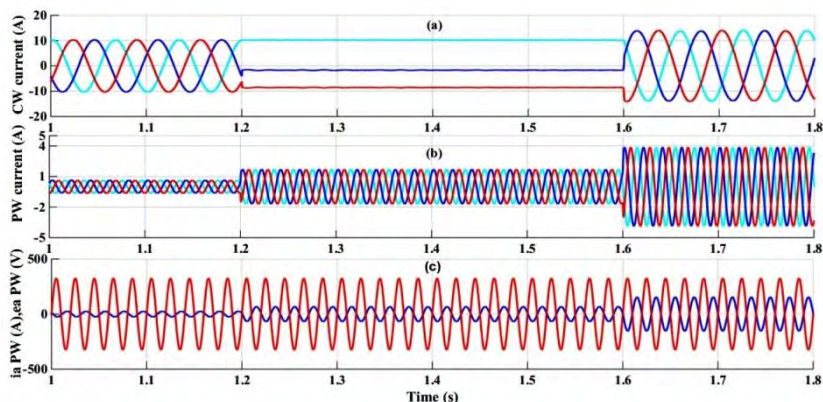


Fig. 16: Simulation results of 'DPC-BDFIG' of 'MSC' under speed step  
 {super-synchronous mode, synchronous mode, sub-synchronous mode}  
 (a) 3-phase current waveform of CW stator; (b) 3-phase current  
 waveform of PW; (c) 1<sup>st</sup> phase a voltage and current of PW

The figure 14a shows the applied wind profile for the studied system, and it could ensure various operation conditions {sub-synchronous mode (525 tr/min), synchronous mode (750 tr/min) and super-synchronous mode (975 tr/min)}. It can be seen, that the generator speed is accurately adjusted to the waveforms of optimal reference speed, which is obtained from MPPT.

The figure 15-b shows the generated active power in case of {sup-synchronous, synchronous and sup-synchronous} operation with zero value of reactive power as can be seen in figure 15c.

The figure 15a and the figure 15b shows the 'PW' stator active and reactive powers with their respective references. The 'PW' stator active power reference is obtained through the MPPT control algorithm. The reference of reactive power of stator 'PW' is set at zero to ensure a unit power factor in order to optimize the quality of the energy transmitted to the grid.

As well can note that the measured active and reactive powers of the 'BDFIG' follow their references perfectly which means that a good steady state performance has been achieved. It is worth to mention, the mode of operation is dictated by the sign of the active power. This last is negative because the machine acts as a generator.

During transient speed changes, it is observed that the active power can successfully track the reference value with high dynamic performance which demonstrates pretty good transient state performance. Meanwhile, reactive power remains uninfluenced as shown in figure 15c, demonstrating excellent decoupling control of active and reactive power.

So briefly, the proposed strategy provided an excellent dynamic behavior under a step change and it is noticed that the coupling effect between the active and reactive power is practically unobservable.

The passage from different operation mode {sub-synchronous to synchronous to super-synchronous} speed is observed to be smooth without any transients in the CW and PW stator current waveforms as shown in figure 16.

The figure 16a and the figure 16b show the CW rotor current and PW stator current. The PW stator current has a sinusoidal shape and with shifting phase at about 180°.

The frequency of 'CW' rotor current is changed according to the rotor speed. For example to maintain a zero frequency for 'CW' rotor current, the 'BDFIG' machine have to rotate at natural speed {750 tr/m, (1.2 s to 1.6 s)}, in the other hand stator current frequency is independent to the rotor speed and it is depending only to the grid frequency.

The magnitude of 'PW' stator current and 'CW' rotor current are varied in accordance with the wind speed changes and corresponding to the amount of active power PW.

**5.1.2 Simulation result of (DPC-GSC) SOGI flux Estimator**

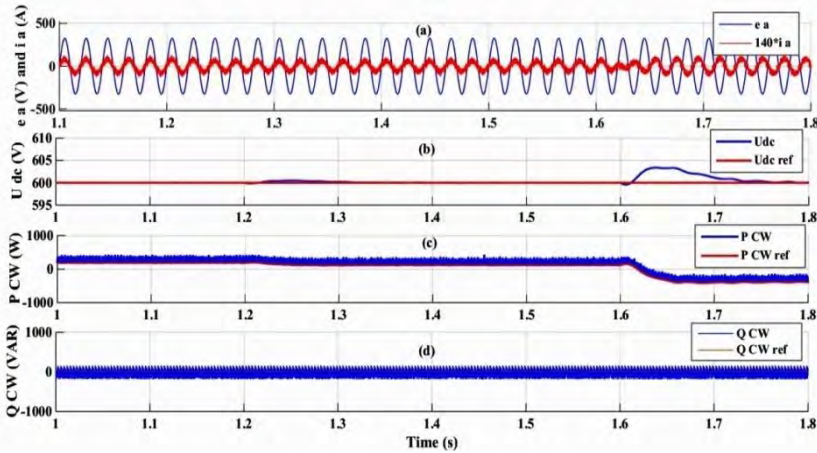


Fig. 17: Simulation results of 'VF-DPC' based 'SOGI-FLL' flux estimation of 'GSC' under speed step {super-synchronous mode, synchronous mode, sub-synchronous mode}; (a) 1<sup>st</sup> voltage and current of GSC; (b) DC-link voltage; (c) active power of GSC; (d) reactive power of GSC

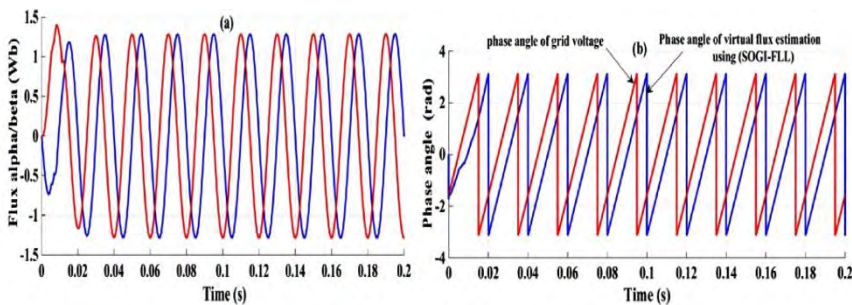


Fig. 18: Virtual flux and Phase angle estimated by 'SOGI-FLL', (a) Virtual flux; (b) comparison of the angle between grid voltage and virtual flux estimated

The figure 17a presents the waveforms of the grid phase voltage and GSC current. It can be seen from this figure that the line currents are very close to a sine-wave. During time interval of (t=1s to 1.6 s), the waveforms of grid current and voltage are exactly in accordance to phase, which explains that the 'CW' stator of 'BDFIG' absorbs active power from the grid during sub-synchronous and synchronous modes, whereas, during time span of (t=1.6s to 1.8 s), the waveforms of 'GSC' current and voltage are in

opposition of phase, so that the 'CW' stator of 'BDFIG' provides active power to the grid {hyper-synchronous mode}.

The figure 17c-d show active and reactive powers of 'GSC'. It can be seen that active power has been varied as well corresponding to the GSC current which means depending to operation mode. The reactive power is set equal to zero to ensure a unit power factor operation and as in PW side reactive power regulation remains unaffected, demonstrating perfect decoupling control feature of active and reactive powers.

The figure 17b presents the waveform of the DC link voltage. The DC link voltage reference is set to 600 V, the measured voltage perfectly follows the reference signal with the exception of the initial conditions where the voltage control loop does not have enough time to react, at 1.6s small variation of DC-Link voltage due to the passage of synchronous mode to the sup-synchronous mode.

The figure 18 presents phase shift between grid voltage angle and virtual flux angle estimated using 'SOGI-FLL' method. It can be seen that the phase angle waveform of virtual flux is smooth and stable, at the same time, the phase angle of 'VF' lags behind the grid voltage with 90°. Then the estimated 'VF' can be used to detect the sector used in control of direct power control GSC.

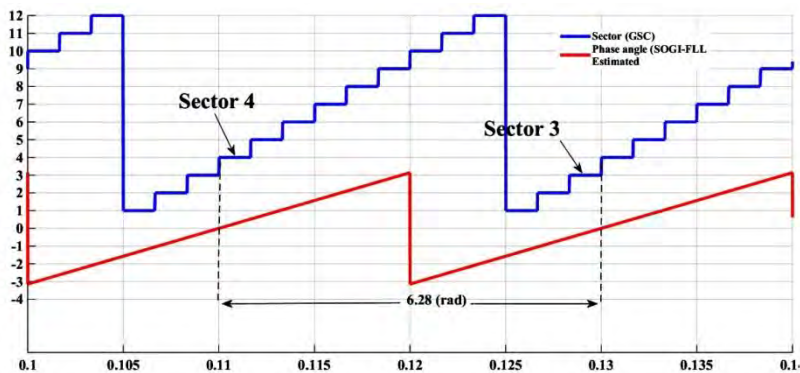


Fig. 19: Phase flux angle and 12 sector of 'VF-DPC' estimated using 'SOGI-FLL'

The figure 19 shows the angle and corresponding sector of virtual flux estimated using 'SOGI-FLL' method. Where can observe that the sector identified using the voltage vector is shifted forward with three ranks when using the virtual flux vector.

## 5.2 Simulation result with variable wind profile

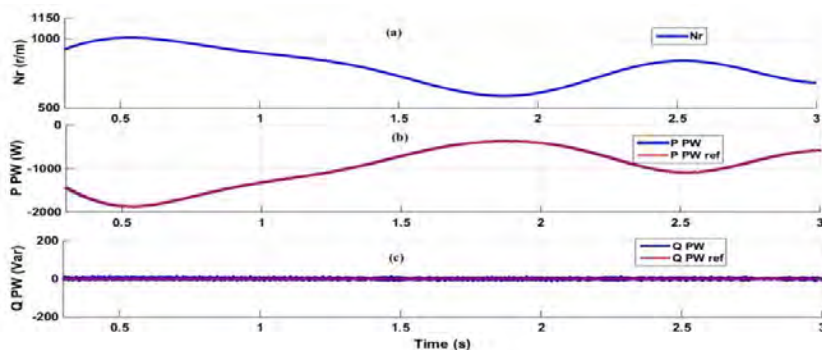


Fig. 20: Simulation results of 'DPC-BDFIG' of MSC under wind speed profile  
(a) Speed; (b) PW active power; (c) PW reactive power

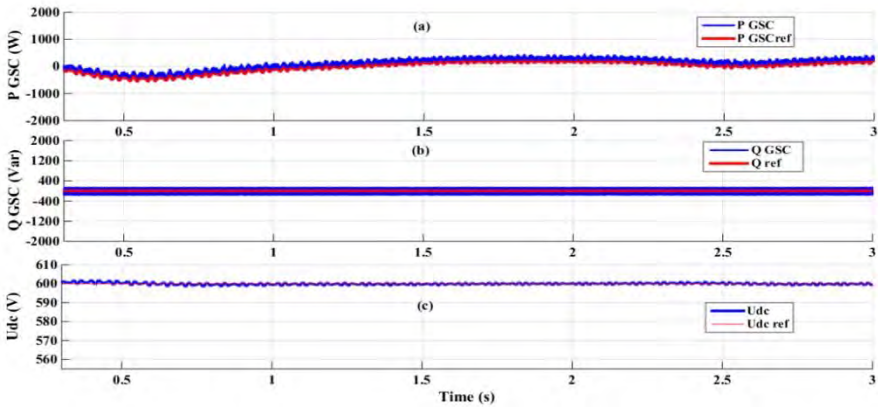


Fig. 21: Simulation results of 'VF-DPC' based 'SOGI-FLL' flux estimation of GSC under wind speed profile (a) Active power (b) Reactive power (c) DC-link voltage

The figure 14b presents the envisaged wind speed profile. The figure 20b-c exhibits the active and reactive powers flow and as in previous section it demonstrates pretty good tracking feature in terms of accuracy and time response.

The figure 21b-c shows the dynamic response of 'BDFIG' with the available generator speed figure 14b. It can be seen, the active and reactive powers of GSC can track their references very well, showing excellent dynamic performance and tracking ability.

The figure 21d shows that the output DC voltage is regulated and it follows the reference voltage command of 600 Volts.

The proposed 'FV-DPC-GSC' and 'DPC-MS' based 'BDFIG' system not only has the good control effect of the power tracking, but also can implement the variable-speed constant-frequency operation.

## 6. CONCLUSION

In this paper, a robust direct power control approach applied for wind energy conversion system 'WECS' based 'BDFIG' machine has been investigated. Mathematical modeling of various parts of the system is introduced and explained. The control process is done in a coordinated manner between grid side and machine side.

Whereas, conventional direct power control has been used for the CW stator side converter in order to adapt and capture the maximum power available by wind turbine to be fed via PW stator to the grid. The maximum power point is defined by an MPPT algorithm which could provide the reference power signal used in the 'DPC PW' stator controller. Meanwhile, grid side control issue focus mainly to ensure constant DC link voltage during system operation and as well ensuring bidirectional power flow between grid and CW stator side.

It is worth to mention that we have been adopted improved direct power control based virtual flux and 'SOGI-FLL' estimator to regulate power flow via grid side converter. Simulation of system has been performed under variable wind profile. Obtained results gave us clear idea about reliability of system in terms of steady state performance and robustness during transients.

Firstly, system could to manage perfectly the main three operation modes {synchronous, sub synchronous and super synchronous speeds} where the power flow

has been transited from mode to another in smoothly way and maintaining reasonable power quality for energy transmitted to the network.

Secondly, test of robustness was conducted using variable wind profile and results demonstrated a pretty good set-point tracking behavior. Finally, the proposed 'FV-DPC-GSC' and 'DPC-MSC' based 'BDFIG' system not just has the great control impact of the power tracking, yet in addition can implement the variable-speed constant-frequency operation.

## REFERENCES

- [1] M. Cheng and Y. Zhu, 'The State of the Art of Wind Energy Conversion Systems and Technologies- A Review', Energy Conversion and Management, Vol. 88, pp. 332 - 347, 2014.
- [2] M. Cheng, X. Wei, P. Han, Y. Zhu, and Z. Chen, 'Modeling and Control of a Novel Dual-Stator Brushless Doubly-Fed Wind Power Generation System', In Proceeding 17<sup>th</sup> International Conference on Electrical Machines and Systems, 'ICEMS', 22 - 25 Oct. 2014
- [3] Shi Jin, Long Shi, Liancheng Zhu, Ting Dong, Fengge Zhang and Wenping Cao, 'Performance Comparison of Direct Power Control for Brushless Doubly-Fed Wind Power Generator with Different Control Winding Structure', in Proceeding 2016 IEEE Transportation Electrification Conference and Expo, Asia-Pacific, 'ITEC Asia-Pacific' 1-4 June 2016.
- [4] J. Hu, J.G. Zhu and D.G. Dorrell, 'A New Control Method of Cascaded Brushless Doubly Fed Induction Generators Using Direct Power Control', IEEE Transactions on Energy Conversion, Vol. 29, N°3, September 2014.
- [5] I. Sarasola, J. Poza, M.A. Rodriguez and G. Abad, 'Direct Torque Control Design and Experimental Evaluation for the Brushless Doubly Fed Machine', Energy Conversion and Management, Vol. 52, pp. 1226 - 1234, 2011.
- [6] P.C. Roberts, R.A. McMahan, P.J. Tavner, J.M. Maciejowski and T.J. Flack, 'Equivalent Circuit for the Brushless Doubly Fed Machine (BDFM) Including Parameter Estimation and Experimental Verification', IEE Proceedings - Electric Power Application, Vol. 152, N°4, pp. 933 - 942, 2005.
- [7] B. Hopfensperger, D.J. Atkinson and R.A. Lakin, 'Stator Flux Oriented Control of a Cascaded Doubly-Fed Induction Machine', IEE Proceedings - Electric Power Applications, Vol. 146, N°6, pp. 597 - 605, Nov. 1999.
- [8] Ming Cheng, Xinchu Wei, Peng Han, Ying Zhu and Zhe Chen, 'Modeling and Control of a Novel Dual-Stator Brushless Doubly-Fed Wind Power Generation System', 17<sup>th</sup> International Conference on Electrical Machines and Systems, ICEMS', 22 - 25 Oct. 2014, Hangzhou, China.
- [9] Sheng Hu and Guorong Zhu, 'A Vector Control Strategy of Grid-Connected Brushless Doubly Fed Induction Generator Based on the Vector Control of Doubly Fed Induction Generator', Applied Power Electronics Conference and Exposition, APEC, 2016 IEEE, 20 - 24 March 2016.
- [10] E. Abdi, R. McMahan, P. Malliband, S. Shao, M. Ezekiel Mathekga, P. Tavner, S. Abdi, A. Oraee, T. Long and M. Tatlow, 'Performance Analysis and Testing of a 250 kW Medium-Speed Brushless Doubly-Fed Induction Generator', IET Renewable Power Generation Vol. 7, N°6, pp. 631 - 638, Nov. 2013.
- [11] J. Poza, E. Oyarbide, I. Sarasola and M. Rodriguez, 'Vector Control Design and Experimental Evaluation for the Brushless Doubly Fed Machine', IET Proceedings Electronic Power Applications, Vol. 3, N°4, pp. 247 - 256, 2009.

- [12] Xinchu Wei, Ming Cheng and Qingsong Wang, 'Direct Power Control Strategies of Cascaded Brushless Doubly Fed Induction Generators', 42<sup>nd</sup> Annual Conference of the IEEE IECON 2016, 23-26 Oct. 2016.
- [13] Kai Ji, Jun Zhu, Yue Gao and Chuan Zeng, 'Vector Control and Synchronization of Brushless Doubly-Fed Machine for High Power Wind Power Generation', 15<sup>th</sup> International Conference of IEEE on Electrical Machines and Systems, 'ICEMS', 21 - 24 Oct. 2012.
- [14] A.R. Prasad, P.D. Ziogas, and S. Manias, 'An Active Power Factor Correction Technique for Three-Phase Diode Rectifiers', IEEE Transactions on Power Electronics, Vol. 6, N°1, pp. 83 – 92, 1991.
- [15] M.P. Kazmierkowski and L. Malesani, 'Current Control Techniques for three-Phase Voltage-Source PWM converters: A survey', IEEE Transactions on Industrial Electronics, Vol. 45, N° 5, pp. 691 –703, 1998.
- [16] V. Pedro and G.D. Marques, 'DC Voltage Control and Stability Analysis of PWM-Voltage-Type Reversible Rectifier', IEEE Transaction on Industrial Electronics, Vol. 45, N°2, pp. 263 – 273, April 1998.
- [17] M. Weinhold, 'A New Control Scheme for Optimal Operation of a Three-Phase Voltage dc Link PWM Converter', in Proceedings International Exhibition and Conference for Power Electronics, Intelligent Motion and Power Quality, 'PCIM Europe 2007'.
- [18] M. Mohseni, S. Islam, and M.A.S. Masoum, 'Enhanced Hysteresis-Based Current Regulators in Vector Control of DFIG Wind Turbines', IEEE Transactions on Power Electronics, Vol. 26, N° 1, pp. 223 – 234, 2011.
- [19] T. Noguchi, H. Tomiki, S. Kondo, and I. Takahashi, 'Direct Power Control of PWM Converter Without Power-Source Voltage Sensors', IEEE Transactions on Industry Applications, Vol. 34, N°3, pp. 473 - 479, 1998.
- [20] M. Malinowski and M. Kazmierkowski, 'Simple Direct Power Control of Three-Phase PWM Rectifier Using Space Vector Modulation aA Comparative Study', European Power Electronics and Drives, Vol. 13, N°2, pp. 27 - 34, 22 Sep 2003.
- [21] Wenshao Bu, Leilei Xu, 'Direct Power Control Strategy of PWM rectifier Based on Improved Virtual Flux-Linkage Observer', Journal of Control Science and Engineering, Vol. 20, 9 p., 2017.
- [22] Marcos B. Ketzler, Cursino B. Jacobina and Sensorless, 'Control Technique for PWM Rectifiers With Voltage Disturbance Rejection and Adaptive Power Factor [JJ]', IEEE Transactions on Industrial Electronics, Vol. 62, N°2, pp. 1140 - 1151, 2015.
- [23] Feng-jiang Wu, Zhi-wen Wang and Li Sub', 'Improved Virtual Flux Oriented Vector Control of PWM rectifier', Journal Electric Machines and Control, Vol. 5, pp. 504 - 508, In Chinese 2008.
- [24] Jon Are Suul, Alvaro Luna, Pedro Rodriguez and T. Undeland, 'Virtual-Flux-Based Voltage-Sensor-Less Power Control for Unbalanced Grid Conditions', IEEE Transactions on Power Electronics, Vol. 27, N°9, 2012.
- [25] R. Zhao, Z. Xin, P.C. Loh and F. Blaabjerg, 'A Novel Flux Estimator Based on SOGI with FLL for Induction Machine Drives', IEEE, Applied Power Electronics Conference and Exposition, 'APEC', 12 May 2016.
- [26] R. Zhao, Z. Xin, P.C.Loh and F. Blaabjerg, 'A Novel Flux Estimator Based on Multiple Second- Order Generalized Integrators and Frequency-Locked Loop for Induction Motor Drives', IEEE Transactions on Power Electronics, Vol. 32, N°8, 2017.
- [27] Z. Xin, R. Zhao, F. Blaabjerg, L. Zhang and P.C. Loh, 'An Improved Flux Observer for Field-Oriented Control of Induction Motors Based on Dual Second-Order Generalized

*Integrator Frequency-Locked Loop*’, IEEE Journal of Emerging and Selected Topics in Power Electronics, Vol. 5, N°1, 2017.

- [28] Siegfried Heier, ‘*Grid Integration of Wind Energy Conversion Systems*’, J. Wiley & Sons Ltd, ISBN 0-471-97143-X, 1998.
- [29] A. Rahab, F. Senani, and H. Benalla, ‘*Direct Power Control of Brushless Doubly-Fed Induction Generator Used in Wind Energy Conversion System*’, International Journal of Power Electronics and Drive System, IJPEDES, Vol. 8, N°1, pp. 417 - 433, 2017.
- [30] S. Jin, F.G. Zhang, Y. Li and Y.X. H1, ‘*Robust Control for VSCF Brushless Doubly-Fed Wind Power Generator System*’, In: Proceeding of the IEEE international Conference on Automation and Logistics, pp. 471–475, Shenyang, China, 2009.
- [31] B. Li and S. Liu, ‘*Study on Direct Torque Control Strategy of Brushless Doubly-Fed Induction Generator for Wind Power Generation*’, Journal of Computational System, Vol. 10, N°24, pp. 599 - 608, 2005.
- [32] M. Malinowski, M.P. Kazmierkowski, S. Hansen, F. Blaabjerg and G.D. Marques, ‘*Virtual-Flux Based Direct Power Control of Three-Phase PWM Rectifiers*’, IEEE Transactions on Industry Applications, Vol. 37, N°4, pp. 1019 - 1027, July-August 2001.